Materials Chemistry and Physics 295 (2023) 127086

Contents lists available at ScienceDirect

Materials Chemistry and Physics

journal homepage: www.elsevier.com/locate/matchemphys

Strong and weak ferromagnetic of cobalt ferrite: Structural, magnetic properties and reflection loss characteristic

Akmal Johan [a,*], Dedi Setiabudidaya [a], Fitri Suryani Arsyad [a], Ramlan [a], Wisnu Ari Adi [b,**]

[a] Department of Physics, Faculty of Mathematics and Natural Sciences, Sriwijaya University, Indralaya, South Sumatra, 30862, Indonesia
[b] Research Center for Advanced Material, National Research and Innovation Agency, Kawasan Puspiptek Serpong, Tangerang Selatan, Banten, Indonesia

GRAPHICAL ABSTRACT

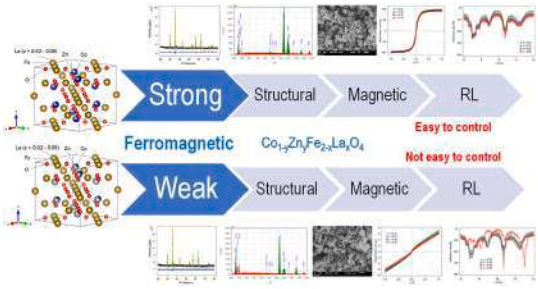

ARTICLE INFO

Keywords:
Cobalt ferrite
Ferromagnetic
Structure
Magnetic
Reflection loss

ABSTRACT

In this research, we investigated the effect of strong and weak ferromagnetic cobalt zinc ferrite dopant ion La^{3+} on the reflection loss characteristics measured at the X-band frequency (8–12 GHz). Strong and weak ferromagnetic cobalt zinc ferrite dopant ion La^{3+} was synthesized by solid state reaction using mechanical milling technique then sintered at 1000 °C for 5 h. Single-phase cobalt ferrite $Co_{0.75}Zn_{0.25}Fe_{2-x}La_xO_4$ and $Co_{0.25}Zn_{0.75}Fe_{2-x}La_xO_4$ (x = 0.02, 0.04, 0.06, and 0.08) with a cubic structure has been successfully formed. Particle morphology and elemental composition have also observed using a scanning electron microscope and energy dispersive spectroscopy, respectively. Meanwhile magnetic properties were characterized by using vibrating sample magnetometer in the form of a hysteresis curve. The presence of Zn in the cobalt ferrite structure that can distinguish between strong and weak ferromagnetic. The results of surface morphology observations show that the sample has a relatively uniform shape and particle size distribution and the results of this elementary analysis show that the phase composition of the two types of samples is in accordance with the expected composition. This research has obtained the most optimum composition and can produce relatively large microwave absorption at the composition of $Co_{0.75}Zn_{0.25}Fe_{2-x}La_xO_4$ with the dopant ion La^{3+}, x = 0.08 with a maximum RL value of −27dB, −25 dB, and −15dB which respectively at the frequencies of 8.4 GHz, 10.2 GHz and 11.2 GHz.

* Corresponding author.
** Corresponding author.
E-mail addresses: akmal_johan@mipa.unsri.ac.id (A. Johan), wisnu.ari.adi@brin.go.id (W.A. Adi).

https://doi.org/10.1016/j.matchemphys.2022.127086
Received 6 September 2022; Received in revised form 14 November 2022; Accepted 22 November 2022
Available online 28 November 2022

1. Introduction

Cobalt ferrite $CoFe_2O_4$ is one of the candidates for microwave absorbing material which has been widely studied because of its excellent performance at high frequencies [1–3]. Besides, cobalt ferrite also has good chemical stability and mechanical hardness [4,5], can increase the degradation resistance [6], a medium coercivity field and is often referred to as a semi-hard magnetic, and a very high saturation magnetization [7,8]. However, all the advantages of these properties are highly dependent on the chemical composition and microstructural characteristics because they can be controlled in the fabrication and synthesis processes as is the case with the hexaferrite system [9]. Considering that cobalt ferrite has good physical and chemical stability, the particle size can be uniform throughout the surface [10]. The permeability and permittivity of the cobalt ferrite complex is capable of being in a very wide frequency range from MHz to GHz. This shows that cobalt ferrite has the potential to be applied as a candidate for microwave absorbers [1].

Cobalt ferrite has a low dielectric loss so that by providing dopant ions that have good permittivity, it is expected to increase the dielectric loss of these materials such as Zn and La [11–13]. The general structure of spinel ferrite is MFe_2O_4, where M is a divalent metal either transition or not, even a combination of these metals as one of the dopant [14,15]. The spinel ferrite structure is described as a tightly packed cubic oxygen atom, where M^{2+} and Fe^{3+} ions can occupy either tetrahedral (A) or octahedral (B) sites, respectively [16–18]. However, this cobalt ferrite ($CoFe_2O_4$) has an inverted spinel structure where under ideal conditions, all Co^{2+} ions are in octahedral sites, and Fe^{3+} ions are evenly distributed between tetrahedral and octahedral sites.

In general, many researches on spinel ferrite have been carried out using various synthesis methods both physically and chemically, such as coprecipitation [19,20], hydrothermal methods [21,22], sol-gel [23], microemulsions [24], mechanical milling [25], citrate gel process [26], irradiation [27] and others [28–32]. Basically, all of these synthesis methods have their respective advantages, but in this study using the solid state reaction method was selected through mechanical milling techniques. The main reason is that if one day this material has a very good performance, especially as a microwave absorbent material and in its application a large-scale material is needed, then this technique becomes the simplest and easiest method. Research on ferrite as a microwave absorbing material is still in great demand to be studied because of its interesting phenomenon. Yunasfi reported that single-phase $NiLa_xFe_{(2-x)}O_4$ samples were successfully synthesized, and doping with lanthanum enhanced the ability to absorb microwaves from 90.01% to 96.61% (reflection loss −14.72 dB at 10.22 GHz) [25]. Recently, the synthesis of zinc-nickel ferrite has also been successfully carried out by Vinnik using solid state reactions and the sol–gel auto combustion technique. They reported that zinc-nickel ferrite is a strong magnet that has the potential to be used in high-frequency applications [33,34]. Several other researchers use rare earth elements as substitution ions in the ferrite structure. Substitution of rare earth metal cations into ferrite structure can cause structural distortion due to the very large difference in ionic radii between transition metal ions and rare earth metal ions, so this can change the magnetic properties and microwave absorption characteristics of the material [11,25,26].

This research is a continuation of previous research related to the synthesis of $Co_{1-x}Zn_xFe_2O_4$ material to increase the permittivity of $CoFe_2O_4$ material which is still relatively low [16], namely by adding the rare earth metal element La into the structure of $Co_{1-y}Zn_yFe_{2-x}La_xO_4$ with several variations of dopant composition. Microwave absorbing materials are required to have wave-like properties in a single phase [35]. This means that the material must have a permeability (magnetic loss) and permittivity (dielectric loss) value. The compatibility ratio with microwaves can be measured based on the impedance value. The content of Zn in the structure of the cobalt ferrite greatly determines the magnetic properties of the material. At the composition Zn = 0.25, the material is still strong ferromagnetic, but at Zn = 0.75, the magnetic properties have changed to near paramagnetic, but still have hysteresis characteristics, so it is called weak ferromagnetic. Thus, the discussion in this study is focused on being able to determine the effect of the substitution of La elements into the cobalt zinc ferrite structure on the structural, magnetic properties and reflection loss characteristics both based on strong and weak ferromagnetic. The results of this study are expected to provide a more comprehensive picture regarding the relationship between microwave absorption and materials based on strong and weak ferromagnetic materials.

2. Experiment method

2.1. Materials and equipment

The raw materials used were CoO powder with a purity of 99.99%, ZnO powder with a purity of >99.99%, Fe_2O_3 powder with a purity of >99%, La_2O_3 powder with a purity of >99%, all them were derived from Sigma-Aldrich products. Meanwhile the synthesis equipment used is High Energy Milling type of PW 1000di Mixer/Mill (HEM) and the characterization equipment used include X-ray diffractometer (XRD) type of Phillips APD 3520, scanning electron microscope and energy dispersive spectroscopy (SEM-EDS) type of JED-430 JEOL, vibrating sample magnetometer (VSM) type of Oxford in the external magnetic field with range of ±1 T at room temperature, and the vector network analyzer (VNA) ADVANTEST R3770 in the frequency range of 8–12 GHz (X-bands frequency).

2.2. Preparation and method

Samples of $Co_{0.75}Zn_{0.25}Fe_{2-x}La_xO_4$ and $Co_{0.75}Zn_{0.25}Fe_{2-x}La_xO_4$ (x = 0.02–0.08) were prepared by solid state reaction using mechanical milling technique with a ratio of 1:1 between the material and the milling balls. The raw materials that have been prepared, namely CoO, ZnO, Fe_2O_3, La_2O_3, and ethanol, are included in 4 vials with a capacity of 20 g each according to the predetermined composition. The composition of $Co_{0.75}Zn_{0.25}Fe_{2-x}La_xO_4$ and $Co_{0.75}Zn_{0.25}Fe_{2-x}La_xO_4$ (x = 0.02–0.08) was calculated based on stoichiometric rules. The mixtures were milled for 5 h, after that the mixtures are dried in the oven for 5 h, and then sintered at a temperature of 1000 °C for 5 h. The results of this sintering process are ground again using mortal agate to remove agglomeration of particles from the sintering process. This fine and dry powder is then carried out several characterizations according to the objectives to be achieved.

3. Results and discussions

3.1. $Co_{0.75}Zn_{0.25}Fe_{2-x}La_xO_4$ (x = 0.02–0.08)

Fig. 1 shows the results of the X-Ray Diffraction pattern analysis for each composition according to the lanthanum dopant content in each sample. The results of the refinement of the X-ray diffraction pattern of the sample $Co_{0.75}Zn_{0.25}Fe_{2-x}La_xO_4$ (x = 0.02–0.08) indicate that the identification of peaks has a single phase of the indicate that the identification of peaks has a single phase of the cobalt ferrite system $CoFe_2O_4$.

The quality of the fitting results from this refinement is very good where the statistical parameters produced are R factor (criteria of fit) and factor S (goodness of fit) or χ^2 (chi-squared) of very small value according to the allowable criteria [36,37]. The structure parameter values, criteria (R factor) and goodness of fit (S) refinement results are shown in Table 1.

Considering that the method used is solid state reaction through mechanical milling technique, and because the substitution of Zn^{2+} and La^{3+} ions can affect the structural distortion which is indicated by the widening of the diffraction peaks, the crystallite size calculation will use

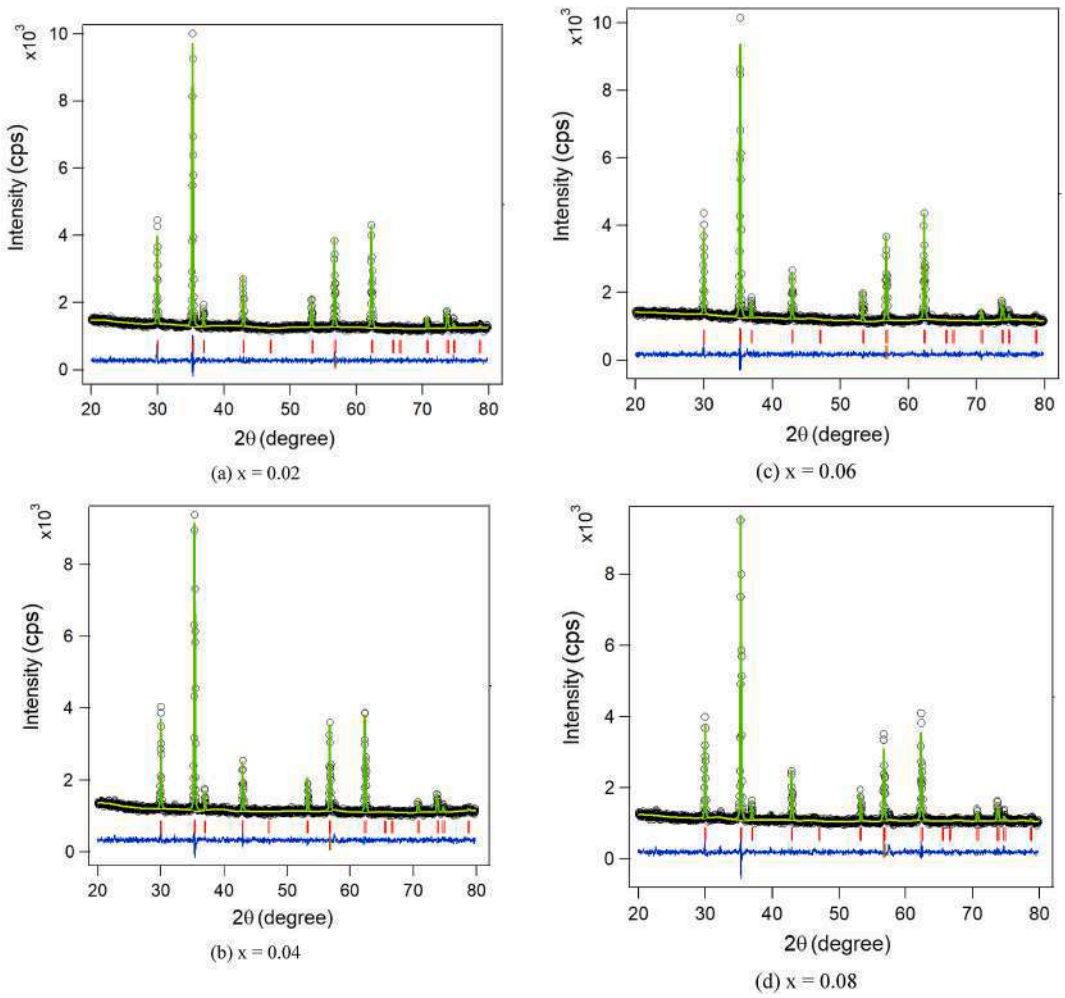

Fig. 1. Refinement of the XRD pattern of the sample $Co_{0.75}Zn_{0.25}Fe_{2-x}La_xO_4$ (x = 0.02–0.08).

Table 1
Structural parameters, criteria and goodness of fit (S) as a result of refinement of the sample $Co_{0.75}Zn_{0.25}Fe_{2-x}La_xO_4$ (x = 0.02–0.08).

x	Phase	SG	R_{wp} (%)	χ^2	Lattice parameters	V	ρ	D
					a = b = c (Å)	(Å^3)	(g/cm^3)	nm
0.02	$CoFe_2O_4$	Fd-3m	2.97	1.256	8.4208(1)	597.12(3)	5.220	46.5
0.04	$CoFe_2O_4$	Fd-3m	3.08	1.290	8.4186(1)	596.65(3)	5.224	47.0
0.06	$CoFe_2O_4$	Fd-3m	3.32	1.415	8.4178(1)	596.49(3)	5.225	47.1
0.08	$CoFe_2O_4$	Fd-3m	3.63	1.590	8.4166(1)	596.22(4)	5.228	47.7

the Williamson-Hall (WH) method [38], where this method assumes that the peak widening is the effect of crystal size (D) and micro-strain (ε) with the given formula:

$$\beta_{hkl}\cos\theta = \frac{K\lambda}{D} + 4\varepsilon\sin\theta \quad (1)$$

where λ is the wavelength (1.5406 Å), β is the full width at half maximum (FWHM) of peaks taking into account the correction factor of the broadening tool, k is the form factor equal to 0.89 and θ is the Bragg reflection angle. The crystallite size calculation technique using the Williamson-Hall (WH) method is to make a linear curve fitting between 4εsinθ as the X axis to βcosθ as the Y axis, resulting in a linear curve equation with constant C. Calculation of the crystallite size is obtained from the value of $C = \frac{K\lambda}{D}$ as shown in Fig. 2 and Table 1.

The particle morphology of the sample $Co_{0.75}Zn_{0.25}Fe_{2-x}La_xO_4$ (x = 0.02–0.08) was observed using a scanning electron microscope (SEM) and the elementary composition analysis was observed using energy dispersive spectroscopy (EDS). This single phase $Co_{0.75}Zn_{0.25}Fe_{2-x}La_xO_4$ has a homogeneous microstructure. Fig. 3 shows the results of observations of the surface morphology of the sample $Co_{0.75}Zn_{0.25}Fe_{2-x}La_xO_4$ (x = 0.02–0.08).

The results of surface morphology observations showed that the sample had a relatively uniform shape and particle size distribution. The average particle size is 200–300 nm for all samples. Observation of the morphology of this sample using the secondary electron method, so that the appearance of the image from the SEM photo is only able to show the homogeneity and uniformity of the shape and size of the particles on the surface of the sample with a magnification of 10,000 times and a reference size of 1 m. In addition, to determine the elemental composition of each sample observed with EDS. The suitability of the stoichiometric composition of the samples and the results of this EDS can be compared. Fig. 4 shows the results of the analysis of the elementary composition of the sample $Co_{0.75}Zn_{0.25}Fe_{2-x}La_xO_4$ (x = 0.02–0.08).

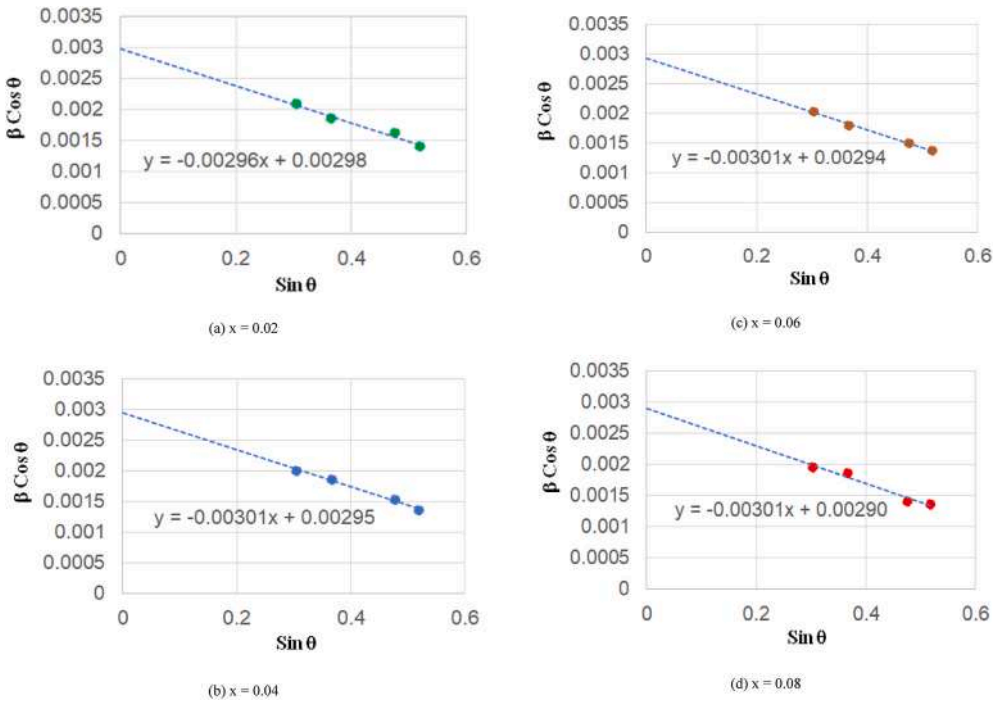

Fig. 2. The results of the calculation of the crystallite size using the WH method of the sample $Co_{0.75}Zn_{0.25}Fe_{2-x}La_xO_4$ (x = 0.02–0.08).

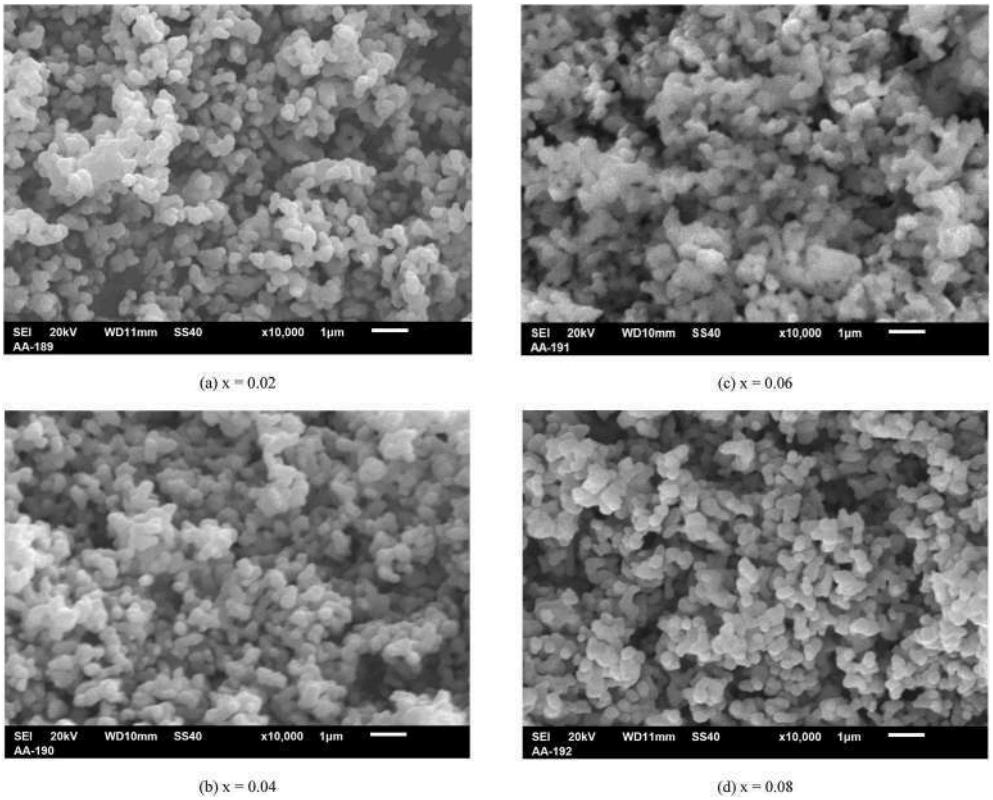

Fig. 3. Surface morphology of the sample $Co_{0.75}Zn_{0.25}Fe_{2-x}La_xO_4$.

In detail, the elemental content in the sample $Co_{0.75}Zn_{0.25}Fe_{2-x}La_xO_4$ is shown in Table 2. And according to the results of this elementary analysis, it is shown that the phase composition of the sample $Co_{0.75}Zn_{0.25}Fe_{2-x}La_xO_4$ is in accordance with the expected composition.

3.2. $Co_{0.25}Zn_{0.75}Fe_{2-x}La_xO_4$ (x = 0.02–0.08)

The X-ray diffraction pattern of the sample $Co_{0.75}Zn_{0.25}Fe_{2-x}La_xO_4$ (x = 0.02–0.08) shown in Fig. 5 was also carried out with quantitative analysis and the refinement results showed that the identification of sample peaks also had a single-phase cobalt ferrite system $CoFe_2O_4$.

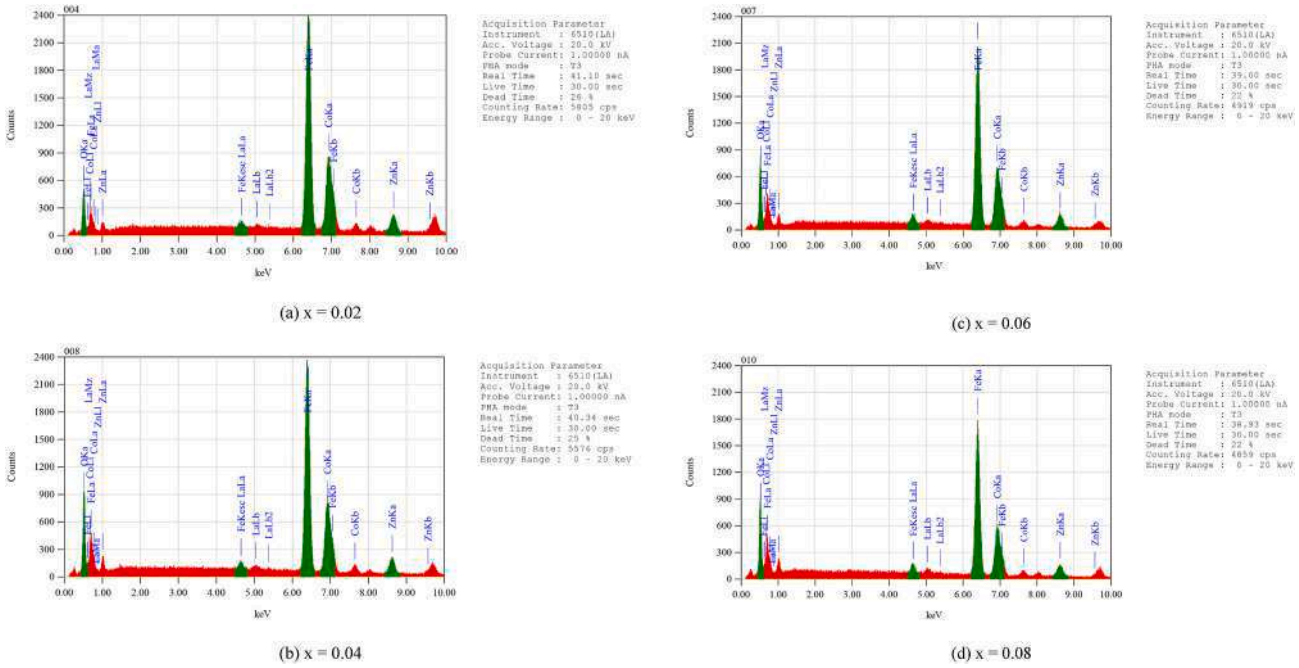

Fig. 4. Elementary analysis of the sample $Co_{0.75}Zn_{0.25}Fe_{2-x}La_xO_4$.

Table 2
Results of compositional analysis using energy dispersive spectroscopy of the sample $Co_{0.75}Zn_{0.25}Fe_{2-x}La_xO_4$ (x = 0.02–0.08).

No.	Element	Content (% Weight)			
		x = 0.02	x = 0.04	x = 0.06	x = 0.08
1.	Oxygen (O)	5.90 ± 0.26	11.09 ± 0.23	10.53 ± 0.22	13.90 ± 0.27
2.	Iron (Zn)	58.37 ± 0.65	54.56 ± 0.58	53.69 ± 0.57	51.94 ± 0.70
3.	Cobalt (Co)	22.73 ± 0.81	21.84 ± 0.72	21.53 ± 0.71	20.99 ± 0.87
4.	Zinc (La)	11.05 ± 0.82	9.98 ± 0.62	10.59 ± 0.60	8.98 ± 0.94
5.	Lanthanum (La)	1.96 ± 0.98	2.53 ± 0.88	3.65 ± 0.86	4.19 ± 0.85

The statistical parameter of the fitting quality is also very good with a very small R factor. Table 3 is the value of the statistical parameter which includes the structure parameter, criteria (R factor) and goodness of fit (S) refinement result.

The result of fitting a linear curve between 4εsinθ to βcosθ produces a linear curve equation with constant C as shown in Fig. 6, so that the size of each crystallite is obtained based on the WH formula and the results are shown in Table 3.

Fig. 7 shows the results of observations of the surface morphology of the sample $Co_{0.25}Zn_{0.75}Fe_{2-x}La_xO_4$ (x = 0.02–0.08) using a scanning electron microscope (SEM) with a magnification of 10,000 times and a reference size of 1 m. The resulting average particle size also ranges from 200 to 300 nm and has a relatively uniform shape and particle size distribution.

The elemental composition of each sample was also observed with EDS and the suitability of the stoichiometric composition of the sample based on the results of this EDS showed that the resulting composition was as expected. Fig. 8 is the result of the analysis of the elementary composition of the sample $Co_{0.25}Zn_{0.75}Fe_{2-x}La_xO_4$ (x = 0.02–0.08).

In detail the elemental content in the sample $Co_{0.25}Zn_{0.75}Fe_{2-x}La_xO_4$ is shown in Table 4, and according to the results of this elementary analysis, it is shown that the phase composition of the sample $Co_{0.25}Zn_{0.75}Fe_{2-x}La_xO_4$ is in accordance with the expected composition. Changes in the phase composition of the sample can affect the quality of its magnetic properties.

All magnetic spinels are derived from magnetite, Fe_3O_4 or $FeO.Fe_2O_3$ systems. The definition is that this magnetic spinel (normal spinel) consists of $[A][B]_2O_4$ or $[FeIII][FeIIIFeII]_2O_4$, which has eight trivalent Fe ions in the A sublattice and a mixture of divalent (eight) and trivalent (eight) ions in the sublattice A. sub-lattice B. In addition, there is also an inverted structure and distribution of cations is referred to as an inverted spinel (inverse spinel form). Simply put, this is an inverted spinel where the form of Fe_2O_3 has a vacancy in the B sublattice.

In this research, 8 divalent Co^{2+} ions have been substituted with Zn^{2+} ions, meaning that some positions of the Co^{2+} site are filled by Zn^{2+} ions, as well as 16 trivalent Fe^{3+} ions have also been substituted with La^{3+} ions where some of the positions of the Fe^{3+} ion site are filled by La^{3+} ions. Fig. 9 shows an illustration of the crystal structure of the cobalt ferrite phase which has been successfully substituted by Zn^{2+} and La^{3+} in the compositions of $Co_{0.75}Zn_{0.25}Fe_{2-x}La_xO_4$, and $Co_{0.25}Zn_{0.75}Fe_{2-x}La_xO_4$.

The illustration in Fig. 9 is the result of an X-ray diffraction pattern analysis using GSAS (general structure analysis system) software and then input data comparisons through phase identification using the MATCH program and referring to the open crystallography database of the cobalt ferrite phase COD: 1533163 [16,39]. The results of this quantitative analysis resulted in changes in structural parameters including the number of occupancy factors of the substituted atoms. The same thing was also done by Trukhanov in determining the atomic occupancy factor using the fullprof program. They reported that the substitution effect was able to change the magnetic and dielectric properties of the material [40,41]. The results of the phase refinement show that the compositions of the two samples $Co_{0.75}Zn_{0.25}Fe_{2-x}La_xO_4$, and $Co_{0.25}Zn_{0.75}Fe_{2-x}La_xO_4$ are single phases with Zn^{2+} and La^{3+} ion substitutions as shown in Figs. 1 and 5. This result can be proven by supporting data from EDS elementary analysis that all samples contain Co, Fe, Zn, and La elements with mass fractions according to the composition of each sample. In the sample composition $Co_{0.75}Zn_{0.25}Fe_{2-x}La_xO_4$ it appears that the elemental content of Co in the mass fraction ranges from 20.99 ± 0.87% to 22.73 ± 0.81%, and the content of the element Zn in the mass fraction ranges from 8.98 ± 0.94% to 11.05 ± 0.82%. Meanwhile, the content of La element in the mass fraction seemed to

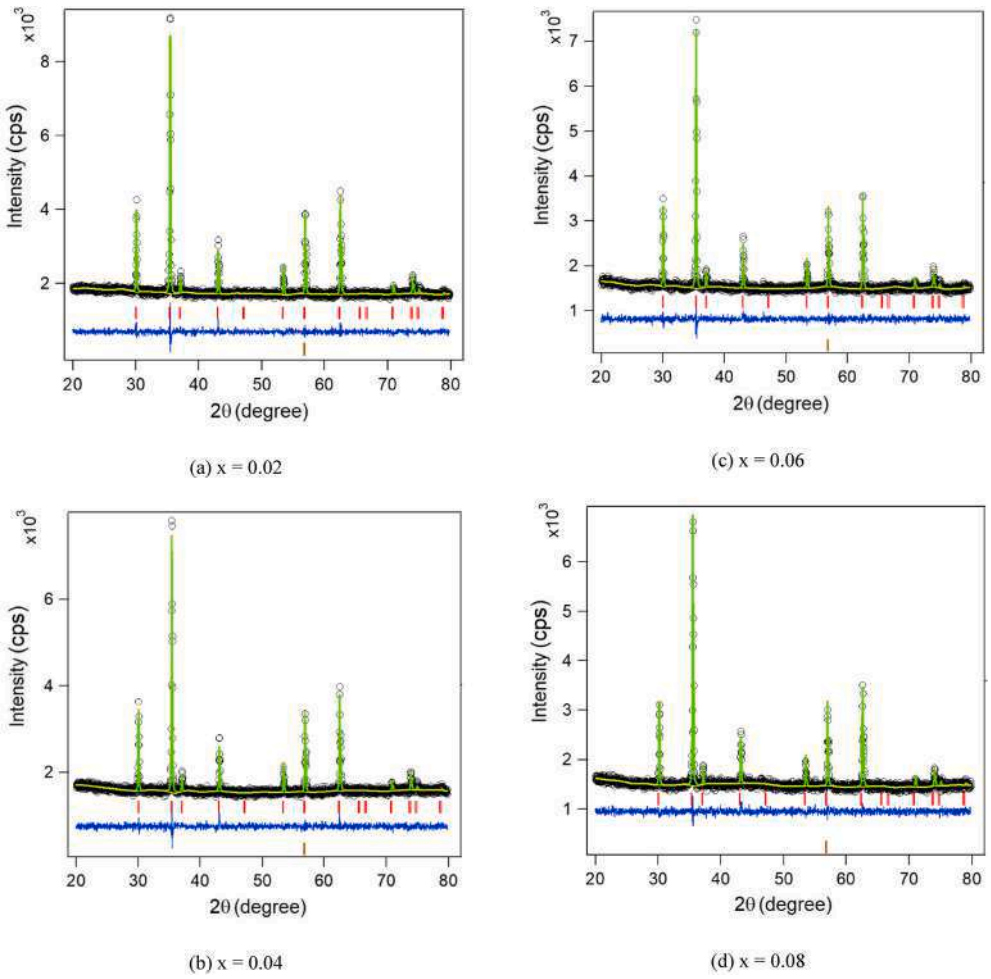

Fig. 5. Refinement of sample XRD pattern $Co_{0.25}Zn_{0.75}Fe_{2-x}La_xO_4$ (x = 0.02–0.08).

Table 3
Parameter structure, criteria and goodness of fit (S) of refinement results of the sample $Co_{0.25}Zn_{0.75}Fe_{2-x}La_xO_4$ (x = 0.02–0.08).

x	Phase	SG	R_{wp} (%)	χ^2	Lattice parameters a = b = c (Å)	V (Å^3)	ρ (g/cm^3)	D nm
0.02	$CoFe_2O_4$	Fd-3m	2.70	1.184	8.3959(2)	591.84(4)	5.266	48.1
0.04	$CoFe_2O_4$	Fd-3m	2.71	1.230	8.3951(2)	591.68(4)	5.268	48.4
0.06	$CoFe_2O_4$	Fd-3m	2.60	1.244	8.3950(1)	591.65(3)	5.268	48.6
0.08	$CoFe_2O_4$	Fd-3m	2.76	1.199	8.3943(2)	591.50(4)	5.269	48.6

increase along with the increase in the composition of x = 0.02 to 0.08 which was 1.96 ± 0.98% to 4.19 ± 0.85%, respectively. In the sample composition $Co_{0.25}Zn_{0.75}Fe_{2-x}La_xO_4$ it appears that the content of Co elements in the mass fraction ranges from 7.16 ± 0.65% to 7.56 ± 0.81%, and the content of Zn elements in the mass fraction ranges from 23.86 ± 0.45% to 25.69 ± 0.82%. Meanwhile, the content of La element in the mass fraction seemed to increase along with the increase in the composition of x = 0.02 to 0.08 which was 1.09 ± 0.88% to 4.57 ± 0.81%, respectively.

The success of this substitution is indicated by a single-phase sample and changes in structural parameters, both unit cell volume and atomic density as shown in Fig. 10.

Fig. 10 shows a decrease in the unit cell volume and an increase in the atomic density of the sample along with the increase in the La^{3+} dopant ion content in each Zn^{2+} dopant ion composition. In this case, the unit cell volume decreases with the doping of La^{3+} ions. This is due to the very large ionic radius of the La^{3+} ion causing this La^{3+} ion to be unable to occupy the tetrahedral and octahedral sites and form aggregates at the grain boundaries. In other words, it is suspected that the cause of the decrease in unit cell volume is the ionic radius that is too large for the La^{3+} ion to cause lattice distortion and produce a level of lattice alignment in the grain boundary region [42,43]. Because the volume of the unit cell decreases as the composition of the La^{3+} dopant ion increases while the atomic number remains constant, the atomic density increases in all sample compositions.

The radius of the La^{3+} ion is much larger than that of the Fe ion, so the La^{3+} ion is generally present at the grain boundaries, which limits grain growth but can induce lattice strains resulting in changes in crystal size and lattice parameters. These microstrains are either due to compression caused by differences in the coefficient of thermal expansion or lattice mismatches between grain and grain boundaries. This condition is reinforced by the results of the calculation of the crystallite size and lattice strain in the three sample compositions as shown in Fig. 11.

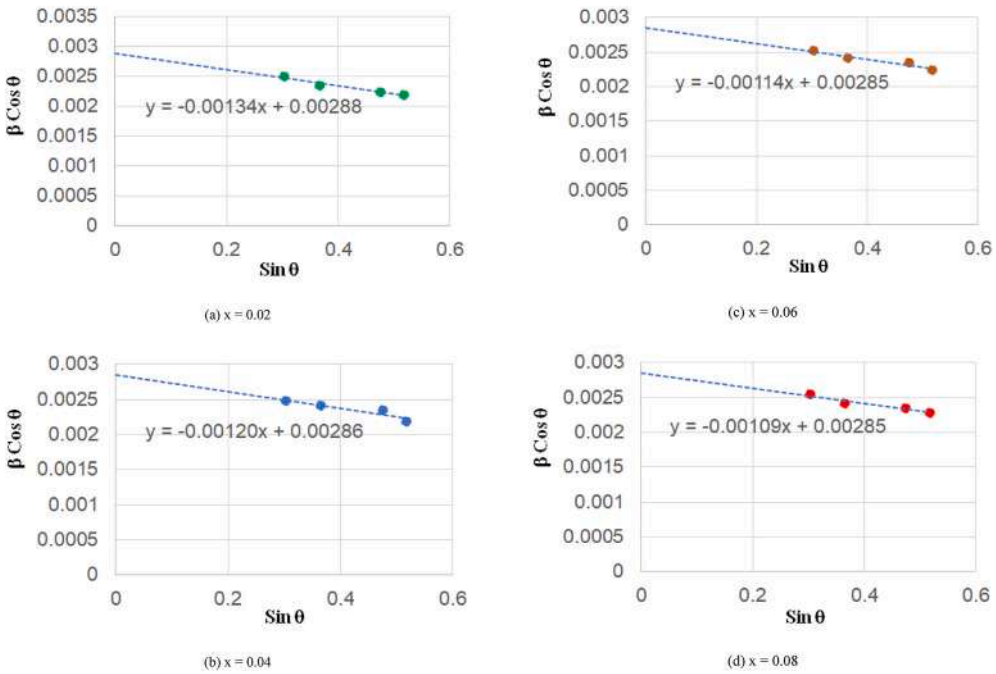

Fig. 6. The results of the calculation of the crystallite size using the WH method of the sample $Co_{0.25}Zn_{0.75}Fe_{2-x}La_xO_4$ (x = 0.02–0.08).

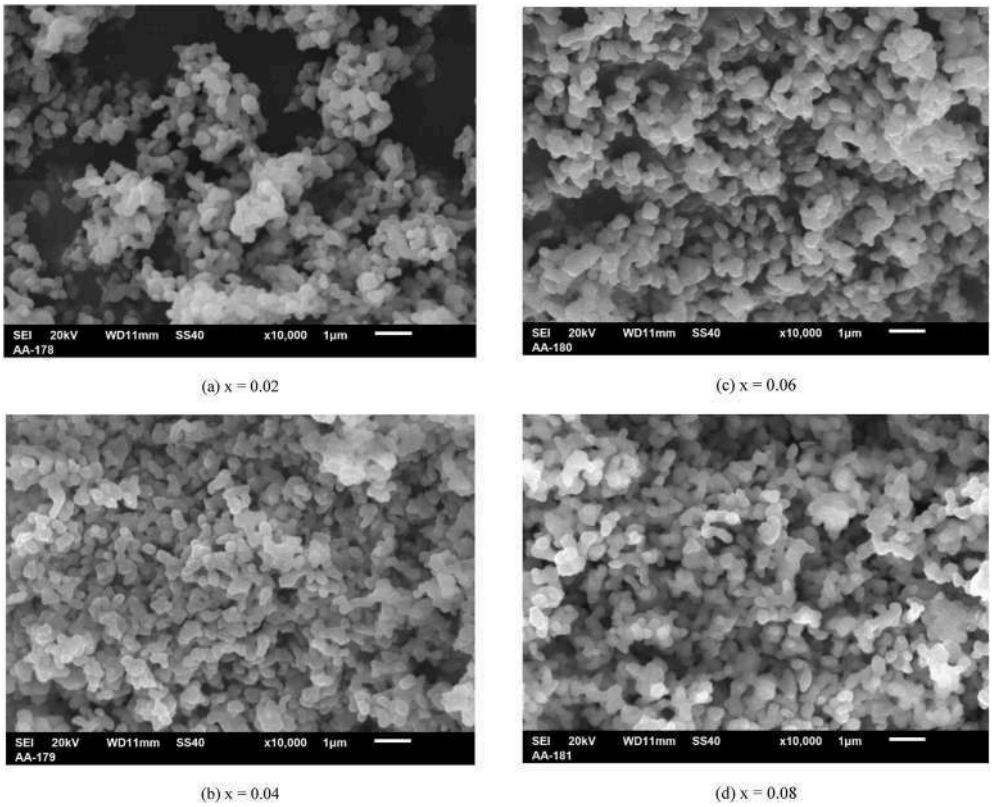

Fig. 7. Surface morphology of the sample $Co_{0.25}Zn_{0.75}Fe_{2-x}La_xO_4$.

What is interesting to discuss here is the effect of increasing crystallite size as the composition of the La^{3+} dopant ion increases. Based on the observations of particle morphology using SEM in Figs. 3 and 7, it is known that the average particle size of each sample composition does not change significantly. In the composition of the samples, both $Co_{0.75}Zn_{0.25}Fe_{2-x}La_xO_4$, and $Co_{0.25}Zn_{0.75}Fe_{2-x}La_xO_4$ it appears that the observed particle size ranges from 200 nm to 300 nm. In this study it appears that the crystallite size increases while the relative particle size does not change, meaning that it is suspected that there is an increase in the magnetic domain area, so that it will affect the magnetic properties of this material.

Magnetism or magnetic properties in this spinel structure arise due to

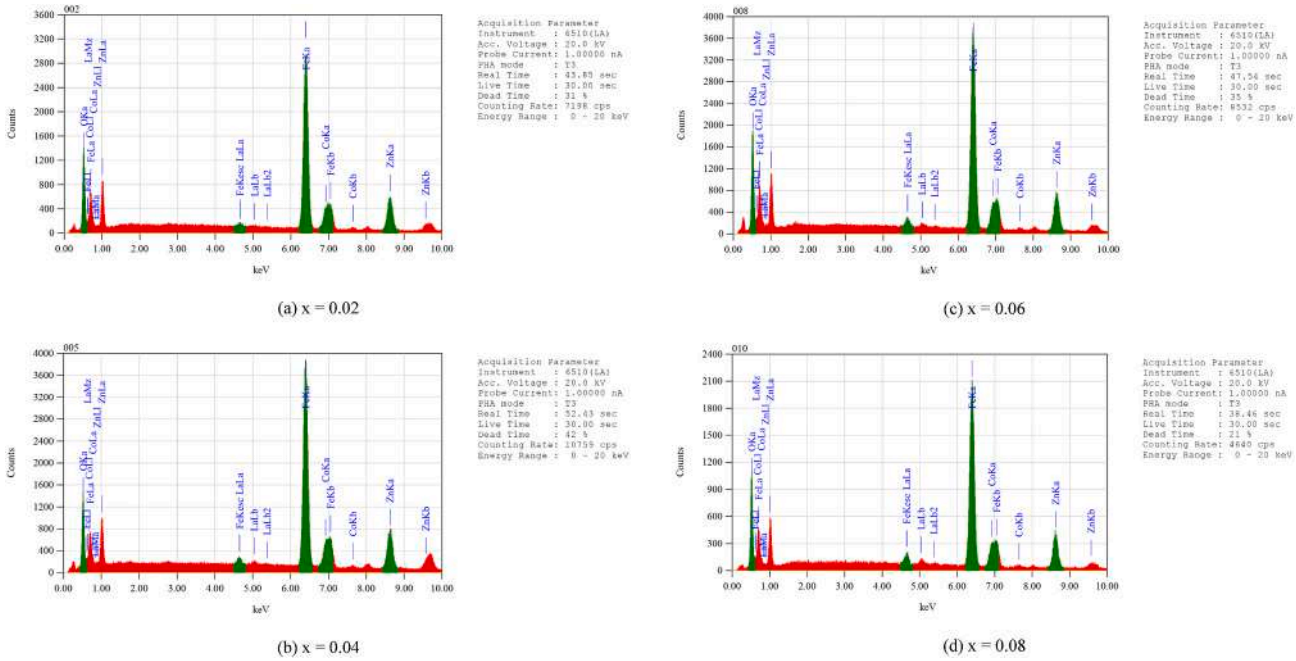

Fig. 8. Elementary analysis of the sample $Co_{0.25}Zn_{0.75}Fe_{2-x}La_xO_4$.

Table 4
Results of compositional analysis using energy dispersive spectroscopy (EDS) of the sample $Co_{0.25}Zn_{0.75}Fe_{2-x}La_xO_4$ (x = 0.02–0.08).

No.	Element	Content (% Weight)			
		x = 0.02	x = 0.04	x = 0.06	x = 0.08
1.	Oxygen (O)	13.38 ± 0.24	10.83 ± 0.23	14.11 ± 0.21	14.25 ± 0.22
2.	Iron (Zn)	52.78 ± 0.57	53.67 ± 0.66	50.94 ± 0.52	50.17 ± 0.53
3.	Cobalt (Co)	7.53 ± 0.70	7.56 ± 0.81	7.52 ± 0.64	7.16 ± 0.65
4.	Zinc (La)	25.22 ± 0.58	25.69 ± 0.82	24.35 ± 0.43	23.86 ± 0.45
5.	Lanthanum (La)	1.09 ± 0.88	2.24 ± 0.11	3.07 ± 0.80	4.57 ± 0.81

superexchange interactions. Fundamentally, superexchange is a negative exchange interaction that results in antialignment of cation spins through the oxygen lattice. This right is the main reason why the magnetization of ferrite is significantly reduced compared to that of most transition metal alloys, such as Fe, Co, Ni, etc., where the unidirectional spin orientation is governed by direct exchange interactions. This is also the reason why it is difficult to increase the magnetization of ferrite materials, because ferrite materials have little flexibility in creating long-range orders of collinear spin at high moments.

On the superexchange, good magnetic interactions between adjacent Fe^{3+} ions are mediated by non-magnetic O^{2-} ions with paired electron spins. In this case, Fe^{3+} is in the 3 d^5 configuration which consists of a t_{2g} orbital (triply degenerate orbital) with a lower energy level and an e_g orbital (excited degenerate orbital) with a higher energy level. Thus the orbitals involved are e_g orbitals (excited degenerate orbitals) which are empty of Fe^{3+} ions and filled 2p orbitals of O^{2-} ions. So the electrons in the 2p orbital of the O^{2-} ion are shared between two adjacent Fe^{3+} ions that fill the empty e_g orbital [44].

Since the spins at site-B and site-A are parallel antiparallel, one increases the net magnetization (M) in the ferrite by creating an imbalance between these sublattice magnetizations. This is generally accomplished by substituting nonmagnetic cations for ferrous ions. The presence of Zn^{2+} substitution for the Co^{2+} site-A cation. causes the magnetization to increase at the expense of the exchange interaction strength AB. This strategy works up to a point, and then the spins on sublattic A and B can no longer rotate due to reduced exchange of sublattice A and B, which ultimately leads to reduced net magnetization. This reduction in net magnetization can be seen based on the results of the hysteresis curve measurements for the three sample compositions as shown in Fig. 12. In addition, some researchers have also linked the presence of oxygen vacancies [45,46] and anion-deficient [47,48] due to this substitution effect. This is related to the electronic properties and magnetotransport of the material.

Fig. 12 shows the results of measuring the magnetic properties of the sample $Co_{1-y}Zn_yFe_{2-x}La_xO_4$ (x = 0.02–0.08). Information data that can be obtained from this hysteresis curve are generally saturation (Ms), remanence (Mr) and coercivity (Hc) fields, all of which are closely related to the magnetic properties of the material. This is indicated by the appearance of the saturation, remanence and coercivity fields of the material as shown in Table 5 and Table 6 for $Co_{0.75}Zn_{0.25}Fe_{2-x}La_xO_4$ and $Co_{0.25}Zn_{0.75}Fe_{2-x}La_xO_4$.

The main indicator of absorption of microwave energy is the value of the reflection loss (RL) where the overall interaction can be represented by the impedance matching of the dielectric and magnetic material (Z_{in}) with the air impedance (Z_o = 377 Ω) as a function of frequency.

With the increase in the concentration of La^{3+} dopant ions, the ferromagnetic properties of the material decrease relatively, especially in the saturation magnetization and coercivity fields. In the sample $Co_{0.75}Zn_{0.25}Fe_{2-x}La_xO_4$ (x = 0.02–0.08), the magnetic parameters both saturation field, remanence, and relative coercivity decreased from 99 emu/gr to 91 emu/gr, from 19 emu/gr to 18 emu/gr, and from 200 Oe to 195 Oe. In the sample $Co_{0.25}Zn_{0.75}Fe_{2-x}La_xO_4$ (x = 0.02–0.08), the magnetic parameters both saturation field and coercivity decreased from 7 emu/gr to 6 emu/gr, and from 80 Oe to 70 Oe, while magnetization relatively constant remanence of 1 emu/gr. The decrease in the coercivity field along with the increase in the La^{3+} dopant ion is thought to come from the decrease in the anisotropy field of each sample. Because when referring to the results of the calculation of the crystallite size as shown in Figs. 2 and 6, it is shown that with increasing crystallite size, it is assumed that the magnetic domain area increases, so it is easier for the external field to direct the magnetic spin in a certain direction depending on the direction of the applied external field. However,

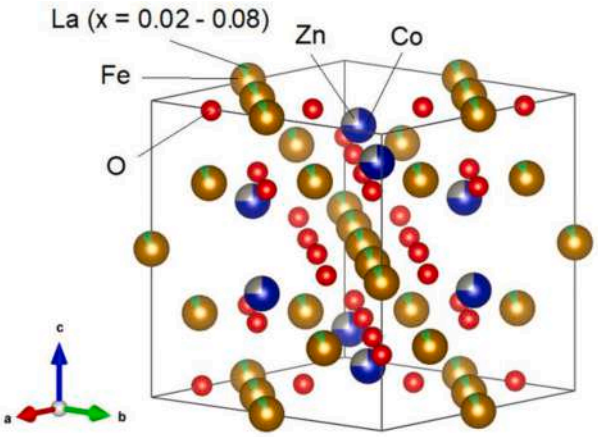

(a) $Co_{0.75}Zn_{0.25}Fe_{2-x}La_xO_4$

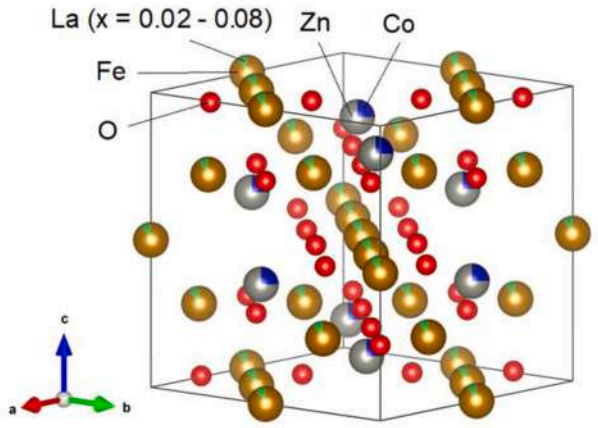

(b) $Co_{0.25}Zn_{0.75}Fe_{2-x}La_xO_4$

Fig. 9. Illustration of the crystal structure of the sample $Co_{1-y}Zn_yFe_{2-x}La_xO_4$.

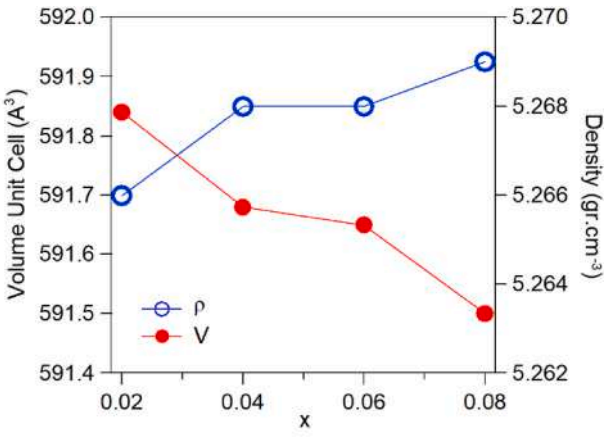

(a) $Co_{0.75}Zn_{0.25}Fe_{2-x}La_xO_4$

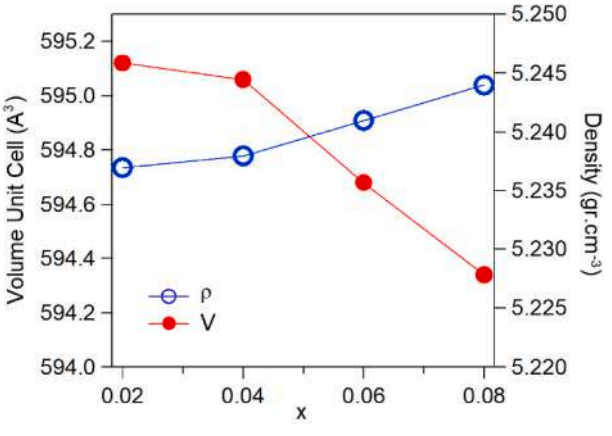

(b) $Co_{0.25}Zn_{0.75}Fe_{2-x}La_xO_4$

Fig. 10. Unit cell volume and atomic density of the sample $Co_{1-y}Zn_yFe_{2-x}La_xO_4$.

specifically for the sample composition $Co_{0.25}Zn_{0.75}Fe_{2-x}La_xO_4$ (x = 0.02–0.08), it appears that there will be a magnetic change or transition from ferromagnetic to paramagnetic, this is very likely to occur because of the phase change of the sample from cobalt ferrite to zinc ferrite, where zinc ferrite behaves paramagnetic at room temperature.

Ultimately the spinel ferrite for each ion type has a thermodynamically preferred lattice distribution based primarily on the cation ionic radius, electrostatic energy, and electronic configuration. This grade of ferrite usually results from nonequilibrium processing such as those involving high kinetic energy transfer (eg, ball milling). Cationic species that exist naturally in some valence states are more susceptible to this type of structure. The tendency to stabilize defects in such structures adds another level of complexity. As one might imagine, determining such a structure with convincing measurement statistics is a significant challenge for experimentalists.

This change in magnetic properties has an impact on the permeability properties of the complex material ($\mu = \mu' + \mu''$), while the presence of Zn and La elements also has an impact on increasing the permittivity of the material complex ($\varepsilon = \varepsilon' + \varepsilon''$). one requirement for materials that have electromagnetic wave absorption properties is that they have high permittivity and permeability to stimulate the occurrence of resonant frequencies. In other words, the characteristics of μ and ε can affect the sensitivity of the material to magnetic and electric fields.

This understanding will be clearer by looking at the results of the reflection loss measurement. Reflection loss (RL) is one indicator to determine the level of microwave absorption of the material, namely the ratio between the incident wave and the reflected wave, and is defined as [49,50]:

$$RL = -20 \log \left| \frac{Z_{in} - Z_0}{Z_{in} + Z_0} \right| \quad (2)$$

If $Z_{in} = Z_o$, then the value of RL will be infinity, meaning no more reflected microwaves. For the one port method, it means that the waves are completely absorbed in the material. Microwave absorption testing using a vector network analyzer (VNA) [51]. The method used is one port. In the one port measurement method [51], the sample must be coated with a metal perfect electrical conductor (PEC) as a perfect reflection material. The sample is in the form of a solid powder which is placed in a VNA holder according to the adapter prepared, namely an adapter with a performance frequency in the X-band. One port method, the incoming wave will only experience two conditions, namely reflected or absorbed. The wave will not be transmitted because it has been coated with a metal plate, so that the microwave does not undergo transmission. Therefore, this one port test can provide real information about the amount of microwave absorption of these materials.

Fig. 13 is the result of measuring the microwave absorption properties in the three sample compositions with the absorption ability indicator marked by a decrease in the value of reflection loss (RL) which means that the more negative RL indicates the greater the microwave absorption rate.

Impedance adjustment is important in the microwave frequency

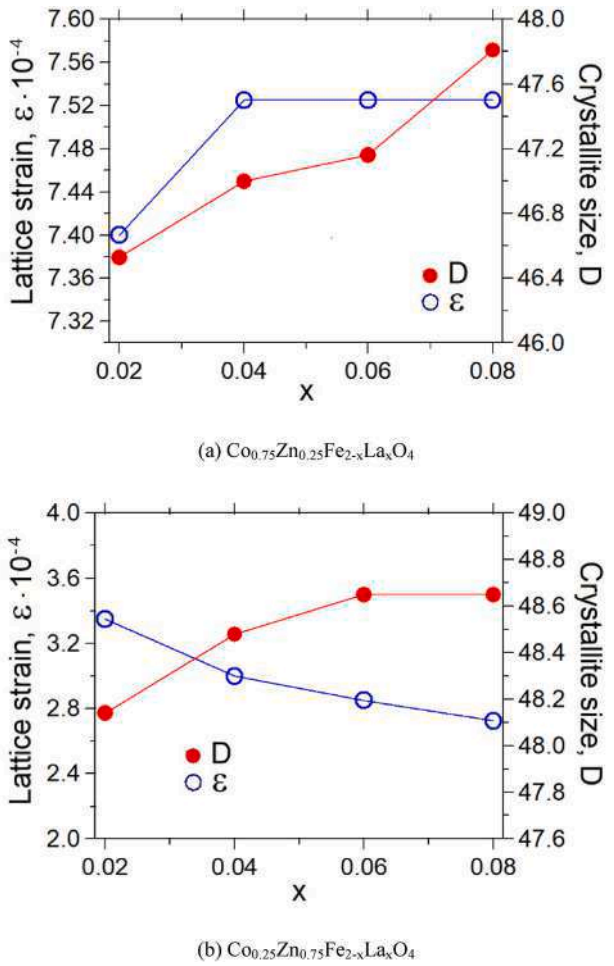

Fig. 11. Crystallite size and lattice strain of the sample $Co_{1-y}Zn_yFe_{2-x}La_xO_4$.

range. Matching has the meaning of providing the same impedance as the characteristic impedance of the microwave. Table 7 shows the results of the RL analysis of the sample $Co_{0.75}Zn_{0.25}Fe_{2-x}La_xO_4$ (x = 0.02–0.08).

Table 8 shows the results of the RL analysis of the sample $Co_{0.75}Zn_{0.25}Fe_{2-x}La_xO_4$ (x = 0.02–0.08). The same thing happened to the results of the RL measurement of the sample with the composition of $Co_{0.25}Zn_{0.75}Fe_{2-x}La_xO_4$ (x = 0.02–0.08) besides finding 3 maximum RL peaks, there was also a shift in the frequency of the absorption peak towards the high frequency which was at a frequency of 8.6 GHz, 10.4 GHz and 11.4 GHz which in the previous composition was at a lower frequency.

In Fig. 13 it is shown that the three sample compositions have relatively the same absorption peaks even though there is a slight shift in frequency and an increase in the value of the reflection loss. In the sample $Co_{0.75}Zn_{0.25}Fe_{2-x}La_xO_4$ (x = 0.02–0.08), three absorption peaks were found based on the results of the sample RL measurements at a frequency of 8.4 GHz, 10.2 GHz and 11.2 GHz where the maximum absorption seemed to increase with the increase in the La^{3+} dopant ion. At a frequency of 8.4 GHz, the maximum RL increased from −25 dB to −27 dB for the dopant ion composition of La^{3+} from 0.02 to 0.08. At a frequency of 10.2 GHz, the maximum RL increased from −19 dB to −25 dB for the dopant ion composition of La^{3+} from 0.02 to 0.08. While at 11.2 GHz frequency, the maximum RL increased from −12 dB to −15 dB also for the dopant ion composition of La^{3+} from 0.02 to 0.08. In general, microwave absorbing materials are affected by the impedance matching between the materials and microwaves through the resonant frequency mechanism. While this resonant frequency is strongly influenced by the

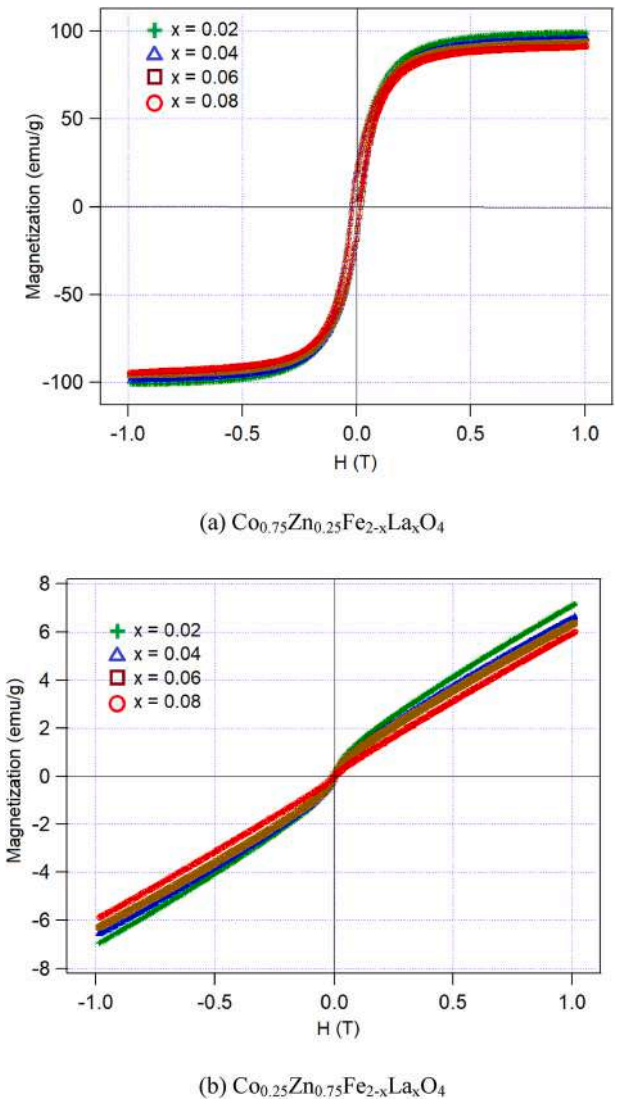

Fig. 12. Hysteresis curve of the sample $Co_{1-y}Zn_yFe_{2-x}La_xO_4$.

Table 5
Magnetic properties of the sample $Co_{0.75}Zn_{0.25}Fe_{2-x}La_xO_4$ (x = 0.02–0.08).

x	Formula	Ms (emu/gr)	Mr (emu/gr)	Hc (Oe)
0.02	$Co_{0.75}Zn_{0.25}Fe_{1.98}La_{0.02}O_4$	99	19	200
0.04	$Co_{0.75}Zn_{0.25}Fe_{1.96}La_{0.04}O_4$	96	18	200
0.06	$Co_{0.75}Zn_{0.25}Fe_{1.94}La_{0.06}O_4$	94	18	200
0.08	$Co_{0.75}Zn_{0.25}Fe_{1.92}La_{0.08}O_4$	91	18	195

Table 6
Magnetic properties of the sample $Co_{0.25}Zn_{0.75}Fe_{2-x}La_xO_4$ (x = 0.02–0.08).

x	Formula	Ms (emu/gr)	Mr (emu/gr)	Hc (Oe)
0.02	$Co_{0.25}Zn_{0.75}Fe_{1.98}La_{0.02}O_4$	7	1	80
0.04	$Co_{0.25}Zn_{0.75}Fe_{1.96}La_{0.04}O_4$	6	1	80
0.06	$Co_{0.25}Zn_{0.75}Fe_{1.94}La_{0.06}O_4$	6	1	80
0.08	$Co_{0.25}Zn_{0.75}Fe_{1.92}La_{0.08}O_4$	6	1	70

degree of ease of magnetic spin of the material polarized by the microwave. There are two factors that affect the level of ease of the interaction, namely the increase in the domain area so that the electron spin resonance mechanism in the domain is easy to occur and the decrease in the anisotropy field in this case is represented by the

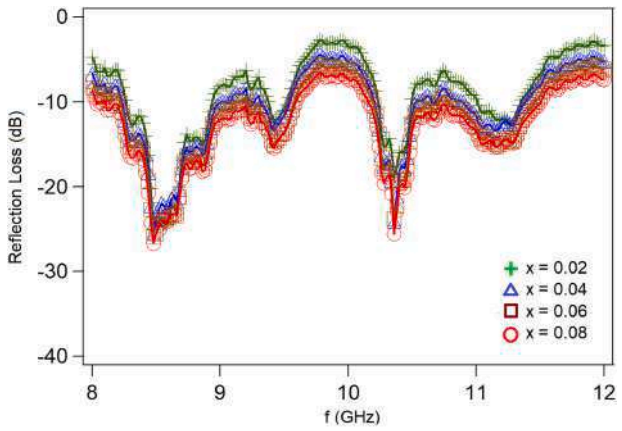

(a) $Co_{0.75}Zn_{0.25}Fe_{2-x}La_xO_4$

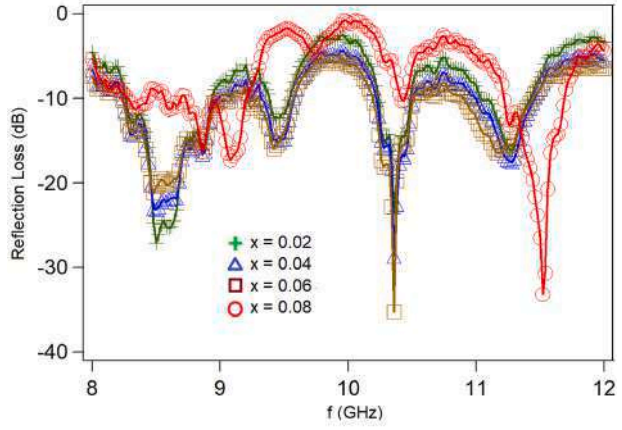

(b) $Co_{0.25}Zn_{0.75}Fe_{2-x}La_xO_4$

Fig. 13. Reflection loss of the sample $Co_{1-y}Zn_yFe_{2-x}La_xO_4$.

Table 7
Refleksion loss (RL) of the sample $Co_{0.75}Zn_{0.25}Fe_{2-x}La_xO_4$ (x = 0.02–0.08).

x	RL (dB)	f (GHz)	RL (dB)	f (GHz)	RL (dB)	f (GHz)
0.02	−25	8.4	−19	10.2	−12	11.2
0.04	−26	8.4	−24	10.2	−13	11.2
0.06	−26	8.4	−24	10.2	−15	11.2
0.08	−27	8.4	- 25	10.2	−15	11.2

Table 8
Refleksion loss (RL) of the sample $Co_{0.25}Zn_{0.75}Fe_{2-x}La_xO_4$ (x = 0.02–0.08).

x	RL (dB)	f (GHz)	RL (dB)	f (GHz)	RL (dB)	f (GHz)
0.02	−25	8.6	−24	10.4	−15	11.4
0.04	−23	8.6	−29	10.4	−17	11.4
0.06	−20	8.6	−35	10.4	−15	11.4
0.08	−15	8.8	−10	10.5	−33	11.6

coercivity field of the material which aims to make the energy needed to polarize the spin. magnetic field in each domain area is getting lower.

This phenomenon can be explained based on the theory of Larmor $f_r = \frac{\gamma H_a}{2\pi}$ which shows that the resonant frequency (f_r) is determined by the gyromagnetic factor (γ) and the anisotropic field (H_a). Meanwhile, the anisotropic field is directly proportional to the anisotropic constant (K_{eff}) and inversely proportional to the magnetic saturation $H_a = \frac{2K}{M_s}$. Therefore, the value of the coercivity field decreases along with the decrease in the anisotropy field of this material. Based on the results of previous studies also showed the same phenomenon that there is a proportional relationship between field coercivity and anisotropic field [52].

Both of these conditions are assumed to be achieved based on XRD and SEM data analysis which shows that the crystallite size of the material increases while the particle size is relatively the same in all dopant ion compositions. This indicates that it is suspected that there is an increase in the domain area, especially in the easy axis, which in turn causes the magnetic spin of the material to move easily due to the presence of microwave photon energy that is able to polarize the magnetic spins of the material. Besides, the second factor is the decrease in the anisotropy field of the material. Based on the results of the analysis of magnetic properties using VSM showed that the coercive field of each composition seemed to decrease with increasing La^{3+} dopant ions. Thus the energy required to polarize the magnetic spins of the material is lower.

Another understanding is that impedance is strongly influenced by the magnitude of the permittivity (ε_r) and permeability (μ_r) of the material. In the case of absorption of microwave energy, the overall interaction can be represented by impedance matching of the dielectric and magnetic materials (Z_{in}) with the air impedance (Z_o) as a function of frequency. This impedance match is very important in relation to the microwave absorption mechanism of the material. A transmission line that is given the same load as the characteristic impedance will have a standing wave ratio (SWR) equal to one, meaning that there is no wave reflection, so that the absorption efficiency becomes optimum if there is no reflected power. If Z_{in} is the same as Z_o, there will be impedance matching. The meaning of this matching is to provide an impedance equal to the characteristic impedance of the microwave. The magnitude of the material impedance is defined as [49,50]:

$$Z_{in} = \sqrt{\frac{\mu_r}{\varepsilon_r}}\tanh\left[j\frac{2\pi fd}{c}\sqrt{\mu_r\varepsilon_r}\right] \quad (3)$$

Where Z_{in}, Z_o, μ_o, ε_o, μ, ε, f, c, and d are the absorber material impedance, microwave impedance in air, air permeability, air permittivity, relative permeability of materials, relative permittivity of materials, frequency, the speed of light, and the thickness of the absorption field. In **Equation (1)** it is stated that the maximum tanh component is 1, so assuming the sample conditions and the performance frequency are the same, the impedance of the material will be directly proportional to the permeability of the complex (μ = μ'+ μ") and inversely proportional to the permittivity of the complex (ε = ε'+ ε"). However, the ratio between permittivity and permeability in materials that have a high absorption rate cannot be determined systematically because it involves the intrinsic properties of a material. However, so far the level of microwave absorption in this material is still not optimal, so that further structural engineering is needed with the existing hypothesis as has been done in this study that the permeability properties of the material can be determined from the properties of the material. It is known that this cobalt ferrite system is a ferromagnetic material that has a very high permeability value because it is believed that both Co^{2+} and Fe^{3+} ions have high Bohr magneton values so that this system will have a very large total magnetic dipole moment. It is evident that based on the results of magnetic properties measurements show that the saturation magnetization of this system material is very large. Meanwhile, the permittivity of the material can be increased by substituting Co^{2+} ions with Zn^{2+} and Fe^{3+} ions with La^{3+} which are believed to have high dielectric constants.

It is the ratio between the permittivity and the permeability of the complex of this material that largely determines the optimum absorption rate that can be achieved. In the sample $Co_{0.25}Zn_{0.75}Fe_{2-x}La_xO_4$ (x = 0.02–0.08), three absorption peaks were also found based on the results of the sample RL measurements at a frequency of 8.6 GHz, 10.4 GHz and 11.4 GHz where the maximum absorption seemed to be relatively decreasing. absorption frequency to a higher frequency. At a frequency

of 8.6 GHz, the maximum RL decreases from −25 dB to −15 dB. At a frequency of 10.4 GHz, the maximum RL increased from −24 dB to −35 dB for the dopant ion composition of La^{3+} from 0.02 to 0.06, while at the composition x = 0.08 it decreased drastically to −10 dB. Meanwhile at the frequency of 11.4 GHz, the maximum RL decreased from −15 dB to −10 dB for the dopant ion composition of La^{3+} from 0.02 to 0.08, while at the composition x = 0.08 there was a shift in the absorption peak at a frequency of 11.6 GHz with a maximum RL of −33 dB. This condition can be explained that in the composition of the sample $Co_{0.25}Zn_{0.75}Fe_{2-x}La_xO_4$ with dopant ion La^{3+}, x = 0.02–0.08, the magnetic properties of this material decrease and a magnetic phase transformation occurs from ferromagnetic to paramagnetic. This means that the permeability of this material complex decreases while the permittivity of the material increases due to the presence of Zn^{2+} and La^{3+} ions. It is suspected that the ratio between permittivity and permeability of the complex produces a smaller impedance so that it is no longer close to the microwave impedance which in turn results in low microwave absorption. Besides, there is a shift in the absorption peak, it is very logical that the higher the permittivity value in the material causes absorption to occur at a higher frequency, considering that based on **Equation (2)** it is stated that the permittivity value ($\varepsilon = \varepsilon' + \varepsilon''$) of the material is directly proportional with the absorption frequency.

The results of this study found the most optimum microwave absorption characteristics at the composition of $Co_{0.75}Zn_{0.25}Fe_{2-x}La_xO_4$ with dopant ion La^{3+}, x = 0.08. Further improvement of absorption ability, several researchers have tried to combine this cubic ferrite system with other microwave absorbing materials such as hexagonal ferrite and studied it to the exchange coupling between the two [53–56]. While in application, the powder of this composition is usually used as a filler which is combined with a polymer in the form of a composite as has been done by Yakovenko. They reported the manufacture of $BaFe_{12-x}Ga_xO_{19}$/epoxy composites based [57,58].

4. Conclusion

Single phase cobalt zinc ferrite system $Co_{0.75}Zn_{0.25}Fe_{2-x}La_xO_4$ and $Co_{0.75}Zn_{0.25}Fe_{2-x}La_xO_4$ with x = 0.02, 0.04, 0.06 and 0.08 has been successfully synthesized to study its correlation with the structural, magnetic properties and microwave absorption characteristics in the 8–12 GHz frequency band (X-band). The particle morphology of all samples were uniform particles with spherical shape and the same relative particle size, but the crystallite size increases as the La^{3+} dopant ion increases. Cobalt zinc ferrite system $Co_{0.75}Zn_{0.25}Fe_{2-x}La_xO_4$ and $Co_{0.75}Zn_{0.25}Fe_{2-x}La_xO_4$ have magnetic behavior respective strong and weak ferromagnetic. The resulting average particle size has a relatively uniform shape and particle size distribution, while the crystallite size is relatively increased but not significant. With increasing concentration of dopant ion La^{3+}, resulted in a relatively decreased ferromagnetic properties of both the cobalt zinc ferrite system $Co_{0.75}Zn_{0.25}Fe_{2-x}La_xO_4$ and $Co_{0.75}Zn_{0.25}Fe_{2-x}La_xO_4$ especially in saturation magnetization and coercivity field. Changes in the structural and magnetic properties of this material result in changes in the absorption characteristics of microwaves. The optimum microwave absorption peak was obtained in the composition $Co_{0.75}Zn_{0.25}Fe_{2-x}La_xO_4$ with the dopant ion La^{3+}, x = 0.08. Microwave absorption in strong ferromagnetic materials is easy to control compared to weak ferromagnetic materials.

CRediT authorship contribution statement

Akmal Johan: Conceptualization, Writing – original draft, Conception and design of study, Acquisition of data, Analysis and/or interpretation of data, Drafting the manuscript, Revising the manuscript critically for important intellectual content, Approval of the version of the manuscript to be published. **Dedi Setiabudidaya:** Conceptualization, Conception and design of study, Analysis and/or interpretation of data, Revising the manuscript critically for important intellectual content, Approval of the version of the manuscript to be published. **Fitri Suryani Arsyad:** Conceptualization, Conception and design of study, Analysis and/or interpretation of data, Approval of the version of the manuscript to be published. **Ramlan:** Conceptualization, Conception and design of study, Analysis and/or interpretation of data, Approval of the version of the manuscript to be published. **Wisnu Ari Adi:** Conceptualization, Writing – original draft, Conception and design of study, Acquisition of data, Analysis and/or interpretation of data, Drafting the manuscript, Revising the manuscript critically for important intellectual content, Approval of the version of the manuscript to be published.

Declaration of competing interest

The authors declare that they have no known competing financial interests or personal relationships that could have appeared to influence the work reported in this paper.

Data availability

No data was used for the research described in the article.

Acknowledgment

The research/publication of this article was funded by DIPA of Public Service Agency of Sriwijaya University 2022. SP DIPA-023.17.2.677515/2022. On December 13, 2021. In accordance with the Rector's Decree Number: 0109/UN9.3.1/SK/2022, On April 28, 2022.

REFERENCE

[1] Y. Yuan, S. Wei, Y. Liang, B. Wang, Y. Wang, Effect of solvothermal reaction-time on microstructure and microwave absorption properties of cobalt ferrite, Materials 13 (2020) 1–15, https://doi.org/10.3390/ma13235331.
[2] A. Poorbafrani, E. Kiani, Enhanced microwave absorption properties in cobalt-zinc ferrite based nanocomposites, J. Magn. Magn Mater. 416 (2016) 10–24, https://doi.org/10.1016/j.jmmm.2016.04.046.
[3] Bi-yu Chen, Ding Chen, Zhi-tao Kang, Ying-zhe Zhang, Preparation and microwave properties of Ni-Co nanoferrites, Journal of Alloyas and Compounds 618 (2015) 222–226, https://doi.org/10.1016/j.jallcom.2014.08.195.
[4] Y.I. Kim, D. Kim, C.S. Lee, Synthesis & Characterization of $CoFe_2O_4$ Magnetic nanoparticles prepared by temperature controlled coprecipitation method, Physica 337 (2003) 42–51, https://doi.org/10.1016/S0921-4526(03)00322-3.
[5] K.K. Senapati, C. Borgohain, P. Phukan, Synthesis of highly stable $CoFe_2O_4$ nanoparticles and their use as magnetically separable catalyst for knoevenagel reaction in aqueous medium, J. Mol. Catal. Chem. 339 (2011) 24–31, https://doi.org/10.1016/j.molcata.2011.02.007.
[6] M.V. Zdorovets, A.L. Kozlovskiy, D.I. Shlimas, D.B. Borgekov, Phase transformations in FeCo - Fe_2CoO_4/Co_3O_4-spinel nanostructures as a result of thermal annealing and their practical application, J. Mater. Sci. Mater. Electron. 32 (2021) 16694–16705, https://doi.org/10.1007/s10854-021-06226-5.
[7] H. Gul, A. Maqsood, Structural, magnetic and electrical properties of cobalt ferrites prepared by the sol-gel route, J. Alloys Compd. 465 (1–2) (2008) 227–231, https://doi.org/10.1016/j.jallcom.2007.11.006.
[8] V. Pillai, D.O. Shah, Synthesis of high-coercivity cobalt ferrite particles using water-in-oil microemulsions, J. Magn. Magn Mater. 163 (1–2) (1996) 243–248, https://doi.org/10.1016/S0304-8853(96)00280-6.
[9] V.A. Turchenko, S.V. Trukhanov, V.G. Kostishin, F. Damay, F. Porcher, D. S. Klygach, M.G. Vakhitov, L.Yu. Matzui, O.S. Yakovenko, B. Bozzo, I. Fina, M. A. Almessiere, Y. Slimani, A. Baykal, D. Zhou, A.V. Trukhanov, Impact of In3+ cations on structure and electromagnetic state of M-type hexaferrites, J. Energy Chem. 69 (2022) 667–676, https://doi.org/10.1016/j.jechem.2021.12.027.
[10] G. Baldi, D. Bonacchi, C. Innocenti, G. Lorenzi, C. Sangregorio, Cobalt ferrite nanoparticles: the control of the particle size and surface state and their effects on magnetic properties, J. Magn. Magn Mater. 311 (1) (2007) 10–16, https://doi.org/10.1016/j.jmmm.2006.11.157.
[11] C. Stergiou, Magnetic, dielectric and microwave absorption properties of rare earth doped Ni-Co and Ni-Co-Zn spinel ferrites, J. Magn. Magn Mater. 426 (2017) 629–635, https://doi.org/10.1016/j.jmmm.2016.11.001.
[12] A. Radon, Ł. Hawełek, D. Łukowiec, J. Kubacki, P. Włodarczyk, Dielectric and electromagnetic interference shielding properties of high entropy (Zn,Fe,Ni,Mg,Cd) Fe_2O_4 ferrite, Sci. Rep. 9 (2019), 20078, https://doi.org/10.1038/s41598-019-56586-6.

[13] H. Xue, Q. Jiao, X. Ni, Y. Wang, H. Li, Q. Wu, et al., Preparation of core-shell Zn doped $CoFe_2O_4$ cubes @CNT composites and their absorbing performances, Micro & Nano Lett. 12 (2017), https://doi.org/10.1049/mnl.2016.0671.

[14] K. Dukenbayev, I.V. Korolkov, D.I. Tishkevich, A.L. Kozlovskiy, S.V. Trukhanov, Y. G. Gorin, E.E. Shumskaya, E.Y. Kaniukov, D.A. Vinnik, M.V. Zdorovets, M. Anisovich, A.V. Trukhanov, D. Tosi, C. Molardi, Fe_3O_4 nanoparticles for complex targeted delivery and boron neutron capture therapy, Nanomaterials 9 (2019) 494, https://doi.org/10.3390/nano9040494.

[15] M.A. Almessiere, A.V. Trukhanov, F.A. Khan, Y. Slimani, N. Tashkandi, V. A. Turchenko, T.I. Zubar, D.I. Tishkevich, S.V. Trukhanov, L.V. Panina, A. Baykal, Correlation between microstructure parameters and anti-cancer activity of the $[Mn_{0.5}Zn_{0.5}](Eu_xNd_xFe_{2-2x})O_4$ nanoferrites produced by modified sol-gel and ultrasonic methods, Ceram. Int. 46 (2020) 7346–7354, https://doi.org/10.1016/j.ceramint.2019.11.230.

[16] A. Johan, W.A. Adi, F.S. Arsyad, D. Setiabudidaya, Analysis crystal structure of magnetic materials Co1-xZnxFe2O4, IOP Conf. Series, J. Phys. Conf. 1282 (2019), 012032, https://doi.org/10.1088/1742-6596/1282/1/012032.

[17] H.L. Andersen, M. Saura-Mu zquiz, C. Granados-Miralles, E. Canevet, N. Lock, M. Christensen, Crystalline and magnetic structure property relationship in spinel ferrite nanoparticles, Nanoscale 10 (2018) 14902–14914, https://doi.org/10.1039/C8NR01534A.

[18] G. Pilania, V. Kocevski, J.A. Valdez, C.R. Kreller, B.P. Uberuaga, Prediction of structure and cation ordering in an ordered normal-inverse double spinel, Commun. Mater. 1 (2020) 84, https://doi.org/10.1038/s43246-020-00082-2.

[19] Y. Qu, H. Yang, N. Yang, Y. Fan, H. Zhu, G. Zou, The effect of reaction temperature on the particle size, structure and magnetic properties of coprecipitated $CoFe_2O_4$ nanoparticles, Mater. Lett. 60 (29–30) (2006) 3548–3552, https://doi.org/10.1016/j.matlet.2006.03.055.

[20] M.P. Gonzalez-Sandoval, A.M. Beesley, M. Miki-Yoshida, L. Fuentes-Cobas, J. A. Matutes-Aquino, Comparative study of the microstructural and magnetic properties of spinel ferrites obtained by co-precipitation, J. Alloys Compd. 369 (1–2) (2004) 190–194, https://doi.org/10.1016/j.jallcom.2003.09.101.

[21] D. Zhao, X. Wu, H. Guan, E. Han, Study on supercritical hydrothermal synthesis of $CoFe_2O_4$ nanoparticles, J. Supercrit. Fluids 42 (2) (2007) 226–233, https://doi.org/10.1016/j.supflu.2007.03.004.

[22] L. Chen, Y. Shen, J. Bai, Large-scale synthesis of uniform spinel ferrite nanoparticles from hydrothermal decomposition of trinuclear heterometallic oxo-centered acetate clusters, Mater. Lett. 63 (12) (2009) 1099–1101, https://doi.org/10.1016/j.matlet.2009.02.034.

[23] H. Gul, A. Maqsood, Structural, magnetic and electrical properties of cobalt ferrites prepared by the sol-gel route, J. Alloys Compd. 465 (1–2) (2008) 227–231, https://doi.org/10.1016/j.jallcom.2007.11.006.

[24] V. Pillai, D.O. Shah, Synthesis of high-coercivity cobalt ferrite particles using water-in-oil microemulsions, J. Magn. Magn Mater. 163 (1–2) (1996) 243–248, https://doi.org/10.1016/S0304-8853(96)00280-6.

[25] Mashadi Yunasfi, A. Mulyawan, W.A. Adi, Synthesis of $NiLa_xFe_{(2-x)}O_4$ system as microwave absorber materials by milling technique, J. Electron. Mater. 49 (2020) 7272–7278, https://doi.org/10.1007/s11664-020-08489-w.

[26] M.A. Almessiere, Y. Slimani, A.V. Trukhanov, A. Baykal, H. Gungunes, E. L. Trukhanova, S.V. Trukhanov, V.G. Kostishin, Strong correlation between Dy^{3+} concentration, structure, magnetic and microwave properties of the $[Ni_{0.5}Co_{0.5}](Dy_xFe_{2-x})O_4$ nanosized ferrites, J. Ind. Eng. Chem. 90 (2020) 251–259, https://doi.org/10.1016/j.jiec.2020.07.020.

[27] A.L. Kozlovskiy, A. Alina, M.V. Zdorovets, Study of the effect of ion irradiation on increasing the photocatalytic activity of WO_3 microparticles, J. Mater. Sci. Mater. Electron. 32 (2021) 3863–3877, https://doi.org/10.1007/s10854-020-05130-8.

[28] Mulyawan A. Yunasfi, Suyanti Mashadi, W.A. Adi, Synthesis of $NiCexFe_{(2-x)}O_4$ ($0 \leq x \leq 0.05$) as microwave absorbing materials via solid-state reaction method, J. Magn. Magn Mater. 532 (2021), 167985, https://doi.org/10.1016/j.jmmm.2021.167985.

[29] V.P.M. Shafi, A. Gedanken, R. Prozorov, J. Balogh, Sonochemical preparation and size-dependent properties of nanostructured $CoFe_2O_4$ particles, Chem. Mater. 10 (11) (1998) 3445–3450, https://doi.org/10.1021/cm980182k.

[30] M. Gharagozlou, Synthesis, characterization and influence of calcination temperature on magnetic properties of nanocrystalline spinel Co-ferrite prepared by polymeric precursor method, J. Alloys Compd. 486 (1–2) (2009) 660–665, https://doi.org/10.1016/j.jallcom.2009.07.025.

[31] S. Singhal, J. Singh, S.K. Barthwal, K. Chandra, Preparation and characterization of nanosize nickel-substituted cobalt ferrites ($Co_{1-x}Ni_xFe_2O_4$), J. Solid State Chem. 178 (10) (2005) 3183–3189, https://doi.org/10.1016/j.jssc.2005.07.020.

[32] Sangmanee, S. Maensiri, Nanostructures and magnetic properties of cobalt ferrite ($CoFe_2O_4$) fabricated by electrospinning, Appl. Phys. A 97 (1) (2009) 167–177, https://doi.org/10.1007/s00339-009-5256-5.

[33] D.A. Vinnik, V.E. Zhivulin, D.P. Sherstyuk, A.Yu. Starikov, P.A. Zezyulina, S. A. Gudkova, D.A. Zherebtsov, K.N. Rozanov, S.V. Trukhanov, K.A. Astapovich, A.S. B. Sombra, D. Zhou, R.B. Jotania, C. Singh, A.V. Trukhanov, Ni substitution effect on the structure, magnetization, resistivity and permeability of zinc ferrites, J. Mater. Chem. C 9 (2021) 5425–5436, https://doi.org/10.1039/D0TC05692H.

[34] D.A. Vinnik, V.E. Zhivulin, D.P. Sherstyuk, A.Yu. Starikov, P.A. Zezyulina, S. A. Gudkova, D.A. Zherebtsov, K.N. Rozanov, S.V. Trukhanov, K.A. Astapovich, V. A. Turchenko, A.S.B. Sombra, D. Zhou, R.B. Jotania, C. Singh, A.V. Trukhanov, Electromagnetic properties of zinc-nickel ferrites in frequency range of 0.05-10 GHz, Mater. Today Chem. 20 (2021), 100460, https://doi.org/10.1016/j.mtchem.2021.100460.

[35] A. Johan, W.A. Adi, F.S. Arsyad, D. Setiabudidaya, Effect of lanthanum substituted CoFe2-xLaxO4 on change of structure parameter and phase formation, Key Eng. Mater. 855 (2020) 70–77. https://doi.org/10.4028/www.scientific.net/kem.855.70.

[36] B.H. Toby, R.B. Von Dreele, GSAS II the genesis of an open-source all-purpose crystallography software package, J. Appl. Crystallogr. 46 (2013) 544–549, https://doi.org/10.1107/S0021889813003531.

[37] M. Sobri Idris, R.A.M. Osman, Structure refinement strategy of Li-based complex oxides using GSAS-EXPGUI software package, Adv. Mater. Res. 795 (2013) 479–482. https://doi.org/10.4028/www.scientific.net/AMR.795.479.

[38] D. Nath, F. Singh, R. Das, X-ray diffraction analysis by Williamson-Hall, Halder-Wagner and size-strain plot methods of CdSe nanoparticles- a comparative study, Mater. Chem. Phys. 239 (2020), 122021, https://doi.org/10.1016/j.matchemphys.2019.122021.

[39] A. Hajalilou, A.M. Saiful, S. Kamyar, A comparative study of differet concentrations of pure Zn powder effects on synthesis, structure, magnetic and microwave absorbing properties in mechanically-alloyed Ni-Zn ferrite, J. Phys. Chem. Solid. 2016 (2016) 96–97, https://doi.org/10.1016/j.jpcs.2016.05.001, 49 – 59.

[40] S.V. Trukhanov, T.I. Zubar, V.A. Turchenko, An.V. Trukhanov, T. Kmjec, J. Kohout, L. Matzui, O. Yakovenko, D.A. Vinnik, A.Yu. Starikov, V.E. Zhivulin, A.S. B. Sombra, D. Zhou, R.B. Jotania, C. Singh, A.V. Trukhanov, Exploration of crystal structure, magnetic and dielectric properties of titanium-barium hexaferrites, Mater. Sci. Eng. B 272 (2021), 115345, https://doi.org/10.1016/j.mseb.2021.115345.

[41] V.A. Turchenko, S.V. Trukhanov, V.G. Kostishin, F. Damay, F. Porcher, D. S. Klygach, M.G. Vakhitov, D. Lyakhov, D. Michels, B. Bozzo, I. Fina, M. A. Almessiere, Y. Slimani, A. Baykal, D. Zhou, A.V. Trukhanov, Features of structure, magnetic state and electrodynamic performance of SrFe12-xInxO19, Sci. Rep. 11 (2021), 18342, https://doi.org/10.1038/s41598-021-97684-8.

[42] P. Samoila, L. Sacarescu, A. Borhan, D. Timpu, M. Grigoras, N. Lupu, M. Zaltariov, V. Harabagiu, Magnetic properties of nanosized Gd doped Ni-Mn-Cr ferrites prepared using the sol-gel autocombustion technique, J. Magn. Magn Mater. 378 (2015) 92–97, https://doi.org/10.1016/j.jmmm.2014.10.174.

[43] M.K. Kokare, N.A. Jadhav, Y. Kumar, K.M. Jadhav, S.M. Rathod, Effect of Nd^{3+} doping on structural and magnetic properties of $Ni_{0.5}Co_{0.5}Fe_2O_4$ nanocrystalline ferrites synthesized by sol-gel auto combustion method, J. Alloys Compd. (2018), https://doi.org/10.1016/j.jallcom.2018.03.168.

[44] P.W. Anderson, Antiferromagnetism, theory of superexchange, Phys. Rev. 79 (1950) 2, https://doi.org/10.1103/PhysRev.79.350.

[45] S.V. Trukhanov, V.V. Fedotova, A.V. Trukhanov, S.G. Stepin, H. Szymczak, Synthesis and structure of nanocrystalline La0.50Ba0.50MnO3, Crystallogr. Rep. 53 (2008) 1177–1180, https://doi.org/10.1134/S1063774508070158.

[46] D.I. Shlimas, A.L. Kozlovskiy, M.V. Zdorovets, Study of the formation effect of the cubic phase of LiTiO2 on the structural, optical, and mechanical properties of Li2 ±xTi1±xO3 ceramics with different contents of the X component, J. Mater. Sci. Mater. Electron. 32 (2021) 7410–7422, https://doi.org/10.1007/s10854-021-05454-z.

[47] S.V. Trukhanov, A.V. Trukhanov, H. Szymczak, Effect of magnetic fields on magnetic phase separation in anion-deficient manganite $La_{0.70}Sr_{0.30}MnO_{2.85}$, Low Temp. Phys. 37 (2011) 465–469, https://doi.org/10.1063/1.3614412.

[48] A. Kozlovskiy, K. Egizbek, M.V. Zdorovets, M. Ibragimova, A. Shumskaya, A. A. Rogachev, Z.V. Ignatovich, K. Kadyrzhanov, Evaluation of the efficiency of detection and capture of manganese in aqueous solutions of $FeCeO_x$ nanocomposites doped with Nb_2O_5, Sensors 20 (2020) 4851, https://doi.org/10.3390/s20174851.

[49] W.A. Adi, Mashadi Yunasfi, D.S. Winatapura, A. Mulyawan, Y. Sarwanto, Y. E. Gunanto, Y. Taryana, Book: Electromagnetic Fields and Waves, Metamaterial: Smart Magnetic Material for Microwave Absorbing Material, Publisher IntechOpen, UK, 2019, pp. 158–176, https://doi.org/10.5772/intechopen.84471.

[50] B.S. Guru, H.R. Hiziroglu, Electromagnetic Field Theory Fundamentals, China Machine Press, Beijing, 2002, pp. 36–60.

[51] R.J. Collier, A.D. Skinner, Microwave Measurement, third ed., Peter Peregrinus Ltd, London, 2007, pp. 1–36.

[52] S. Kumar, S. Supriya, R. Pandey, L.K. Pradhan, R.K. Singh, M. Kar, Effect of lattice strain on structural and magnetic properties of Ca substituted barium hexaferrite, J. Magn. Magn Mater. 458 (2018) 30–38, https://doi.org/10.1016/j.jmmm.2018.02.093.

[53] N.A. Algarou, Y. Slimani, M.A. Almessiere, A. Sadaqat, A.V. Trukhanov, M. A. Gondal, A.S. Hakeem, S.V. Trukhanov, M.G. Vakhitov, D.S. Klygach, A. Manikandan, A. Baykal, Functional $Sr_{0.5}Ba_{0.5}Sm_{0.02}Fe_{11.98}O_4$/x $(Ni_{0.8}Zn_{0.2}Fe_2O_4)$ hard-soft ferrite nanocomposites: structure, magnetic and microwave properties, Nanomaterials 10 (2020) 2134, https://doi.org/10.3390/nano10112134.

[54] M.A. Almessiere, S. Güner, Y. Slimani, M. Hassan, A. Baykal, M.A. Gondal, U. Baig, S.V. Trukhanov, A.V. Trukhanov, Structural and magnetic properties of $Co_{0.5}Ni_{0.5}Ga_{0.01}Gd_{0.01}Fe_{1.98}O_4/ZnFe_2O_4$ spinel ferrite nanocomposites: comparative study between sol-gel and pulsed laser ablation in liquid approaches, Nanomaterials 11 (2021) 2461, https://doi.org/10.3390/nano11092461.

[55] M.A. Almessiere, Y. Slimani, N.A. Algarou, M.G. Vakhitov, D.S. Klygach, A. Baykal, T.I. Zubar, S.V. Trukhanov, A.V. Trukhanov, H. Attia, M. Sertkol, I.A. Auwal, Tuning the structure, magnetic and high frequency properties of Sc-doped $Sr_{0.5}Ba_{0.5}Sc_xFe_{12-x}O_{19}/NiFe_2O_4$ hard/soft nanocomposites, Adv. Electr. Mater. 8 (2022), 2101124, https://doi.org/10.1002/aelm.202101124.

[56] M.A. Almessiere, N.A. Algarou, Y. Slimani, A. Sadaqat, A. Baykal, A. Manikandan, S.V. Trukhanov, A.V. Trukhanov, I. Ercan, Investigation of exchange coupling and microwave properties of hard/soft $(SrNi_{0.02}Zr_{0.01}Fe_{11.96}O_{19})/(CoFe_2O_4)_x$

nanocomposites, Mater, Today Nano 18 (2022), 100186, https://doi.org/10.1016/j.mtnano.2022.100186.

[57] O. Yakovenko, O. Lazarenko, L. Matzui, L. Vovchenko, M. Borovoy, P. Tesel'ko, O. Lozitsky, K. Astapovich, A. Trukhanov, S. Trukhanov, Effect of Ga content on magnetic properties of $BaFe_{12-x}Ga_xO_{19}$/epoxy composites, J. Mater. Sci. 55 (2020) 9385–9395, https://doi.org/10.1007/s10853-020-04661-z.

[58] O.S. Yakovenko, L.Yu. Matzui, L.L. Vovchenko, V.V. Oliynyk, A.V. Trukhanov, S. V. Trukhanov, M.O. Borovoy, P.O. Tesel'ko, V.L. Launets, O.A. Syvolozhskyi, K. A. Astapovich, Effect of magnetic fillers and their orientation on the electrodynamic properties of $BaFe_{12-x}Ga_xO_{19}$ (x = 0.1-1.2)-epoxy composites with carbon nanotubes within GHz range, Appl. Nanosci. 10 (2020) 4747–4752, https://doi.org/10.1007/s13204-020-01477-w.